Passivity-Based Control of Single-Loop Grid-Forming Inverters

Akhavan, Ali; Vasquez, Juan C.; Guerrero, Josep M.

Published in:
IEEE Journal of Emerging and Selected Topics in Industrial Electronics

DOI (link to publication from Publisher):
10.1109/JESTIE.2022.3232027

Publication date:
2023

Document Version
Accepted author manuscript, peer reviewed version

Passivity-Based Control of Single-Loop Grid-Forming Inverters

Ali Akhavan, *Senior Member, IEEE*, Juan C. Vasquez, *Senior Member, IEEE*, and Josep M. Guerrero, *Fellow, IEEE*

***Abstract*- This paper addresses the passivity-based control of grid-forming inverters with an emphasis focused on the single-loop control system. It is elaborated that the closed-loop control system could be stabilized even without damping the resonance of the *LC* filter, and just by introducing the negative phase to the system. This negative phase is introduced using an all-pass filter that is adopted in series with the voltage regulator, and therefore, the system structure keeps its simplicity. It is also revealed that, unlike the traditional single-loop control system in which the stability region is higher than one-third of the sampling frequency, the proposed method is able to widen the stability region to frequencies lower than one-sixth of the sampling frequency. Then, the output impedance of the inverter is modified using the feedback of the output current to have a passive behavior up to the Nyquist frequency, which assures the stability of the system in different grid impedances and load conditions. The controller design procedure is elaborated in each part to provide the passivity of the system. The proposed control system is examined by experimental tests in grid-tied and off-grid modes to validate the theoretical concepts.**

***Index Terms*— Grid-forming inverters, output impedance, passivity, single-loop control system, stability.**

I. Introduction

Grid-forming inverters (GFIs) have the unique capability of working in both grid-tied and off-grid modes. This characteristic makes them one of the interesting choices in developing microgrids, where it allows the microgrid to take advantage of working in two modes [1]. In this way, the microgrid can switch between off-grid and grid-tied modes smoothly [2]. On the other hand, GFIs are able to support the weak grids to keep the voltage and frequency within the acceptable range. Taking these advantages, however, needs a well-designed control system. The linear control scheme, as a straightforward solution, could be divided into two categories, which are single- and double-loop control systems [3], [4].

The double-loop control approaches basically consist of an inner inductor current loop, and an outer loop that is used to control the capacitor voltage. It has been revealed that the inner loop acts as a virtual impedance, which in turn improves the stability of the system by mitigation of the *LC* filter resonance [5]. However, it is well known that the virtual impedance highly depends on the system and control parameters, as well as the delay that comes from the pulse-width modulation and sampling [6].

The effect of the delay is to the extent that it makes the real part of the virtual impedance negative in frequencies higher than one-sixth of the sampling frequency (f_s/6) [7]. Thus, when the resonance of the *LC* filter is higher than f_s/6, the virtual impedance not only does not mitigate the resonance, but also destabilizes the system because it exhibits negative resistance property. Even though several approaches that are mostly based on delay compensation have been proposed to extend the stability region of the virtual impedance, however, they normally complicate the control system design procedure. Adopting high-pass, band-pass, and notch filters [8]-[10], and also, an observer-based method [11] are some examples of delay negative effect compensation. On the other hand, these methods partially compensate for the delay effect, therefore, they can be hardly used as a general method for systems with different parameters.

Despite having a positive virtual resistance at the resonance frequency, there is no guarantee for the stability of the system in different grid impedance and load conditions as besides the stability of the closed-loop system, the behavior of the output impedance of the inverter affects the system stability [12]. Passivity is a concept that deals with the stability of both closed-loop and output impedance at the same time [13]. It reveals that to guarantee the stability of an inverter while it is operating in different load and grid impedance conditions, the stability of the closed-loop system is not the only constraint. Besides, the output impedance of the inverter should be passive in all or at least a wide range of frequencies. In other words, the phase of the output impedance should be in the range of [-90°, 90°]. All of these factors show that designing a control system may have additional challenges.

The single-loop control schemes, on the other hand, just have a voltage control loop. Therefore, designing the controller is much easier than the dual-loop scheme. However, there is no loop for mitigation of the *LC* filter resonance. Unlike double-loop control systems in which the delay degrades the stability of the system, the introduced negative phase by the delay improves the system stability if a proper control bandwidth is designed for the system [14].

Even though it has been proved that the single-loop control system could be designed stably thanks to the delay effect when the resonance frequency is higher than f_s/3 [15], however, a resonance damping mechanism is still needed when the resonance frequency does not meet the aforementioned constraint. This is the main drawback of the

This work was supported by the VILLUM FONDEN under the VILLUM Investigator Grant 25920, Center for Research on Microgrids (CROM).

The authors are with the AAU Energy, Aalborg University, Aalborg, Denmark (e-mail: alak@energy.aau.dk; juq@energy.aau.dk; joz@energy.aau.dk).

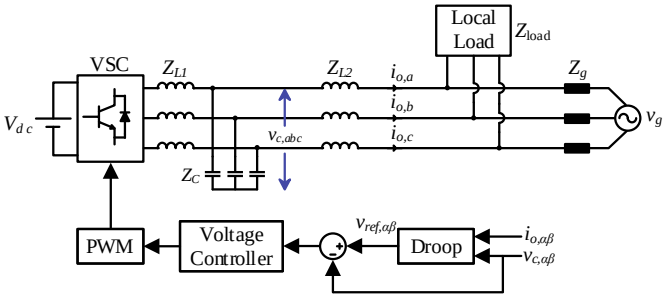

Fig. 1. The structure of a single-loop GFI.

single-loop control system, which leads to more interest in dual-loop control systems. The passive damping method is the soundest choice to solve this problem, however, it inevitably increases the power losses, and consequently, decreases the system efficiency [16]. Therefore, an improved control system is needed that on the one hand keeps the simple structure of the single-loop control system, but on the other hand, extends the stability region of the control system without passive damping resonance mitigation. To this end, a pole placement-based method is proposed in [17], which is simple, yet sensitive to the tolerances of parameters. In [14], different voltage regulators including proportional, resonant, and proportional-resonant-integrator regulators are employed, and the stability regions of their corresponding control systems are investigated. Then, the effects of the different discretization methods are elaborated in each case. However, the output impedance of the inverter is not studied, and its effect on stability is overlooked.

To take advantage of the single-loop control system, this paper develops a control system based on the passivity for single-loop GFIs. The system stably works without any passive damping mechanisms even when the resonance frequency is far lower than $f_s/3$. The proposed method is based on the negative phase injection by using an all-pass filter which is adopted in series with the voltage regulator. Thus, the closed-loop system could be stabilized while it keeps its single-loop structure, and thus, the system control design procedure remains reasonably simple. Afterward, the output impedance of the inverter is reshaped to act passively. To this end, the feedback of the inverter output current is employed, which brings the passivity to the system for the frequencies up to the Nyquist frequency. It, in turn, ensures the stability of the system while the inverter interacts with different loads and grid impedances.

This paper elaborates on the passivity-based control of single-loop GFIs as follows. In Section II, the system structure and the basic control system, as well as the related challenges of the single-loop scheme are thoroughly explained. Then, the stability region of the closed-loop system is extended in Section III. The output impedance of the inverter is reshaped in Section IV to make the system passive. The validation of the proposed method and theoretical analysis is done in Section V in both grid-tied and off-grid modes using an experimental setup. The conclusion of the paper is summarized in Section VI.

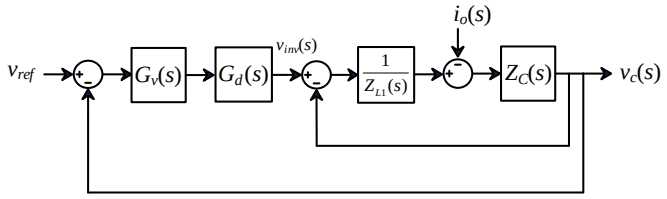

Fig. 2. The control block diagram of a single-loop GFI.

II. System Description and Stability Analysis

Fig. 1 illustrates the diagram of a GFI, in which an *LCL* filter at the output of the inverter mitigates the high-order switching harmonics. Z_{L1}, Z_{L2}, and Z_C are impedances of the *LCL* filter, which are given by:

$$Z_{L1} = L_1 s,\ Z_{L2} = L_2 s,\ Z_C = \frac{1}{Cs}. \tag{1}$$

The GFI is able to be connected to the grid through the grid impedance Z_g, feed the local load with impedance Z_{load}, or both at the same time.

The droop controller in Fig. 1 generates the reference voltage for the internal voltage control loop. Its effect can be overlooked when the voltage control loop is analyzed from the stability point of view since its dynamics are normally much slower than the internal loop [14], [18]. Therefore, the block diagram of the control system could be derived as shown in Fig. 2, in which, $G_v(s)$ is the voltage regulator, and $G_d(s)$ is the continuous model of the delay [19] with the sampling time of T_s as follows:

$$G_d(s) = e^{-1.5T_s s} \tag{2}$$

Regarding Fig. 2, the impedance Z_{L2} has no effect on the stability of the closed-loop system. However, it needs to be considered as a part of grid/load impedance, which its effect on the stability of the system will be explored in Section IV, where the passivity-based stability is elaborated.

The loop gain of the control system $T(s)$ could be achieved by referring to Fig. 2 as

$$T(s) = G_v(s)G_d(s)\frac{\omega_r^2}{s^2+\omega_r^2} \tag{3}$$

where ω_r is the angular resonance frequency of the inverter-side inductor and filter capacitor.

$$\omega_r = 2\pi f_r = \frac{1}{\sqrt{L_1 C}} \tag{4}$$

Normally, a proportional-resonant (PR) controller is used as the voltage regulator.

$$G_v(s) = k_p + k_r\frac{s}{s^2+2\omega_\alpha s+\omega_0^2} \tag{5}$$

where k_p and k_r are the proportional and resonant coefficients. Also, $\omega_0 = 2\pi f_0$ is the angular fundamental frequency, and ω_α is the bandwidth of $G_v(s)$.

The effect of the resonant term could be disregarded for frequencies that are not near the fundamental frequency [20]. Therefore, the loop gain could be simplified by just considering the proportional term as (6), for analyzing the system stability in the range of medium and high frequencies.

$$T'(s) = k_p G_d(s) \frac{\omega_r^2}{s^2 + \omega_r^2} \tag{6}$$

Regarding (6), the phase and magnitude of the loop gain could be derived in the frequency domain as

$$\angle T'(j\omega) = \begin{cases} -1.5T_s\omega & \omega < \omega_r \\ -\pi - 1.5T_s\omega & \omega > \omega_r \end{cases} \tag{7}$$

$$\left|T'(j\omega)\right| = \frac{k_p}{1 - \left(\frac{\omega}{\omega_r}\right)^2} \tag{8}$$

The resonance is the main reason for the instability of the system. However, if the crossover frequency of the system is smaller than the resonance frequency, the system could work stably by selecting a proper k_p to provide a positive phase margin (PM) and gain margin (GM) for the system. To this end, the phase curve in the Bode diagram of loop gain should cross -180° before the resonance frequency. Therefore, according to (7), the boundary resonance frequency (f_{rb}) in which the system could work stably is derived as:

$$-1.5T_s\omega_{rb} = -\pi \Rightarrow f_{rb} = \frac{\omega_{rb}}{2\pi} = \frac{f_s}{3} \tag{9}$$

According to (9), a stable system could be designed even without damping the filter resonance by a proper k_p if the resonance frequency is higher than $f_s/3$. This characteristic of single-loop GFIs is because of the term $-1.5T_s\omega$ that comes from the delay in (6). In other words, the introduced negative phase of the delay helps the single-loop GFIs to work stably when $f_r > f_s/3$.

Fig. 3 depicts the bode diagrams of loop gain $T(s)$ for the cases in which $f_r < f_s/3$ and $f_r > f_s/3$, and with a similar k_p for both cases. As could be observed, for the case that $f_r > f_s/3$, when the phase plot crosses -180°, the magnitude of the Bode plot is below 0 dB (GM > 0). However, this is not the case when $f_r < f_s/3$, in which GM < 0 because of the resonance peak.

Despite the stability of the single-loop GFIs when $f_r > f_s/3$, however, the system still needs a mechanism to keep its stability when $f_r < f_s/3$. Using the passive damping methods increases the losses. On the other hand, using double-loop systems makes the control system design procedure complicated. Inspiring the effect of the delay on making the single-loop systems stable, an approach will be proposed in the next Section to introduce the negative phase to the system. In this way, the closed-loop system can be stabilized for the resonance frequencies far lower than $f_s/3$.

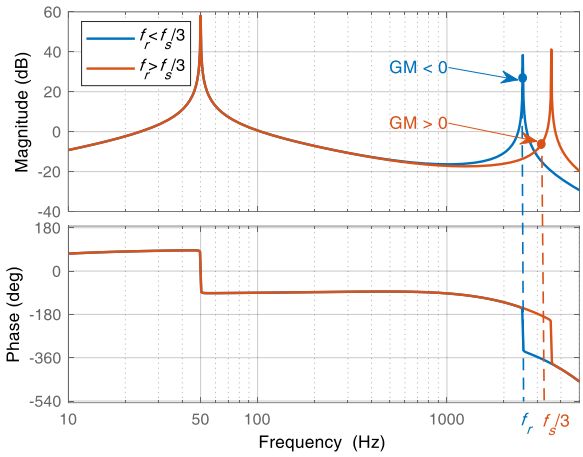

Fig. 3. The Bode diagrams of the system loop gain $T(s)$ for the cases $f_r < f_s/3$ and $f_r > f_s/3$.

III. Widening the Stability Region

It was shown in the previous Section that the single-loop control system could be designed stably if $f_r > f_s/3$ thanks to the negative phase that the delay introduces. Therefore, if a more negative phase is introduced to the system, the stability region of the closed-loop system could be widened. To this end, the first action that could be done is to replace the PR voltage regulator with a pure resonant regulator as follows:

$$G_v(s) = k_r \frac{s}{s^2 + 2\omega_\alpha s + \omega_0^2} \tag{10}$$

The reason behind this action is that the pure resonant regulator behaves as an integral controller (1/s) in the medium and high frequencies [21], and therefore, it introduces -90° to the system. Fig. 4 depicts the Bode diagrams of a resonant regulator with k_r = 1 and an integral controller to show the aforementioned fact intuitively. As could be observed, the Bode diagrams well coincide in the frequencies higher than the fundamental frequency. Thus, the loop gain of the system with a resonant regulator in (11-a), could be simplified as (11-b) in the interesting frequencies for the stability analysis.

$$T(s) = G_d(s) \frac{k_r s}{s^2 + 2\omega_\alpha s + \omega_0^2} \frac{\omega_r^2}{s^2 + \omega_r^2} \tag{11-a}$$

$$T(s) \approx G_d(s) \frac{k_r}{s} \frac{\omega_r^2}{s^2 + \omega_r^2} \tag{11-b}$$

Regarding (11-b), the phase and magnitude of the loop gain could be derived as

$$\angle T(j\omega) = \begin{cases} -\frac{\pi}{2} - 1.5T_s\omega & \omega < \omega_r \\ -\frac{3\pi}{2} - 1.5T_s\omega & \omega > \omega_r \end{cases} \tag{12}$$

$$\left|T(j\omega)\right| = \frac{k_r}{\omega\left[1 - \left(\frac{\omega}{\omega_r}\right)^2\right]} \tag{13}$$

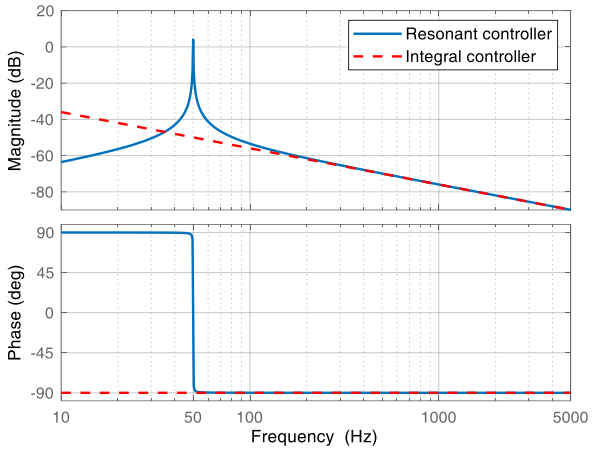

Fig. 4. The Bode diagrams of the resonant and integral controllers.

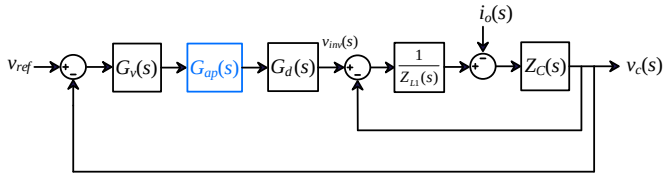

Fig. 5. The control block diagram of the single-loop GFI with an all-pass filter.

According to (12), it could be realized that by using the resonant regulator, the boundary frequency f_{rb} is widened from $f_s/3$ to $f_s/6$ as follows:

$$-\frac{\pi}{2}-1.5T_s\omega_{rb}=-\pi \Rightarrow f_{rb}=\frac{\omega_{rb}}{2\pi}=\frac{f_s}{6} \tag{14}$$

Even though now the system could be designed stably when $f_r > f_s/6$, however, the system is still may be destabilized if $f_r < f_s/6$. Therefore, it is still preferred that the boundary frequency be lowered to widen the stability region. To this end, an all-pass filter is adopted in series with the voltage regulator, as shown in Fig. 5, to introduce a more negative phase to the system. The transfer function of the adopted controller is

$$G_{ap}(s)=k_{ap}\frac{\omega_{ap}-s}{\omega_{ap}+s} \tag{15}$$

where k_{ap} and ω_{ap} are the coefficient and corner frequency of the all-pass filter.

The loop gain of the system by adding the all-pass filter can be simply achieved as follows:

$$T(s)\approx G_d(s)G_{ap}(s)\frac{k_r}{s}\frac{\omega_r^2}{s^2+\omega_r^2} \tag{16}$$

To design the control system, ω_{ap} should be tuned first to provide a robust stability region with respect to the resonance frequency, and then k_{ap} could be tuned to provide a positive and acceptable GM for the system.

The parameters of the system under study are presented in Table I. As could be observed, the resonance frequency f_r is 1250Hz, which is smaller than $f_s/6$. Therefore, the system could not be stabilized just by using a resonant voltage

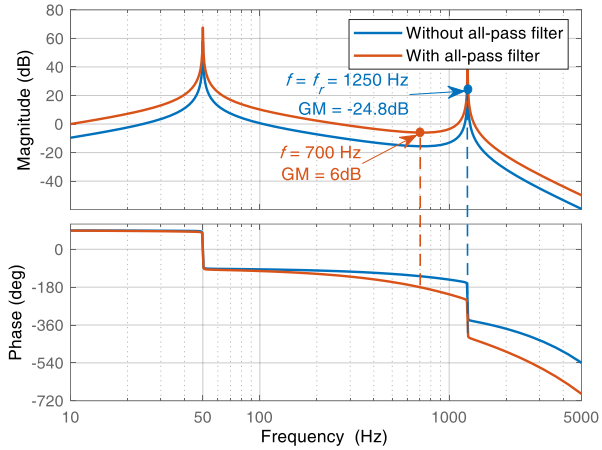

Fig. 6. The Bode diagrams of $T(s)$ with and without the all-pass filter.

regulator. The coefficient of the resonant regulator k_r is tuned so that the system has a high loop gain at the fundamental frequency. Thus, k_r = 500 is chosen. Fig. 6 depicts the Bode diagram of $T(s)$ without the all-pass filter. As can be found, at the resonance frequency where the phase curve crosses -180°, GM < 0 because of the resonance peak, which indicates that the system is unstable in this condition. Therefore, the negative phase should be injected into the system by the all-pass filter, so that the phase crossover frequency in which the phase curve crosses -180°, is smaller than the resonance frequency.

Regarding (16), the phase and magnitude of $T(s)$ are derived as (17) and (18).

$$\angle T(j\omega)=\begin{cases}-\frac{\pi}{2}-1.5T_s\omega-2\tan^{-1}\frac{\omega}{\omega_{ap}} & \omega<\omega_r\\ -\frac{3\pi}{2}-1.5T_s\omega-2\tan^{-1}\frac{\omega}{\omega_{ap}} & \omega>\omega_r\end{cases} \tag{17}$$

$$\left|T(j\omega)\right|=\frac{k_rk_{ap}}{\omega\left[1-\left(\frac{\omega}{\omega_r}\right)^2\right]} \tag{18}$$

The phase crossover frequency should be designed far lower than f_r, to consider the tolerances of system parameters. Therefore, f = 700 Hz is considered in this paper as the phase crossover frequency. In this way, ω_{ap} could be calculated according to (17) as follows:

$$-\frac{\pi}{2}-1.5T_s\omega-2\tan^{-1}\frac{\omega}{\omega_{ap}}\Big|_{\omega=2\pi\times700}=-\pi \tag{19}$$

$$\Rightarrow \omega_{ap}=2\pi\times1429\ (\text{rad/s})$$

After designing ω_{ap}, the coefficient of the all-pass filter k_{ap} could be designed by defining an acceptable GM for the system. By letting GM = 6 dB, k_{ap} could be obtained by using (18) as

TABLE I
SYSTEM PARAMETERS

Inductor L_1	1.8 mH
Capacitor C	9 µF
Resonance frequency of L_1-C	1250 Hz
Inductor L_2	1.8 mH
DC-link voltage, V_{dc}	700 V
Sampling frequency, f_s	10 kHz
Nominal voltage (RMS)	220 V (Phase voltage)
Power frequency	50 Hz
Grid impedance	L_g = 1.8 mH
Load impedance	R_L = 80 Ω || C_L= 30 µF

$$20\log\left.\frac{k_r k_{ap}}{\omega\left[1-\left(\frac{\omega}{\omega_r}\right)^2\right]}\right|_{\omega=2\pi\times700} = -6\,\text{dB} \Rightarrow k_{ap} = 3 \tag{20}$$

The Bode plot of the loop gain with the designed all-pass filter is also illustrated in Fig. 6. It can be seen that the phase crossover frequency is 700 Hz, which shows that the stability region of the closed-loop system has been widened from $f_s/3$ to 700 Hz by using the resonant voltage regulator and all-pass filter. Also, GM = 6 dB, which validates the accuracy of the mathematical derivations and theoretical analysis.

It is worth mentioning that despite the stability of the system, an undamped resonance (see Fig. 6) always may amplify the system noises. In this situation, even though the system remains stable, as there is no right half-plane pole [14], however, it may affect the power quality. This is the main drawback of single-loop control systems. On the other hand, dual-loop control systems could be adopted, in which the main task of the internal loop is damping the resonance by emulating a virtual impedance [5]. In fact, it is a trade-off between the single-loop and dual-loop systems, in which the former provides system simplicity at the cost of noise amplification, and the latter provides system robustness at the cost of complexity.

IV. PASSIVITY ENHANCEMENT

Inverters interact with the grid impedance, loads, and also themselves while they are connected in parallel [22]. Therefore, not only does the stability of the closed-loop transfer function matter, but also the output impedance of the inverter matters since it distinguishes the behavior of the inverter with respect to other components in the system [23]. A grid-forming inverter can be modeled as shown in Fig. 7, which is the Thevenin equivalent circuit of the system. In this figure, $G_{cl}(s)$ and $Z_o(s)$ are the transfer functions of the closed-loop gain and output impedance of the inverter, respectively, which could be derived from the block diagram in Fig. 5.

$$v_c(s) = G_{cl}(s)v_{ref}(s) - Z_o(s)i_o(s) \tag{21}$$

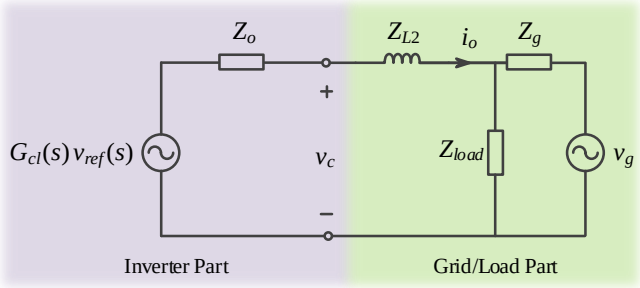

Fig. 7. The Thevenin model of a GFI.

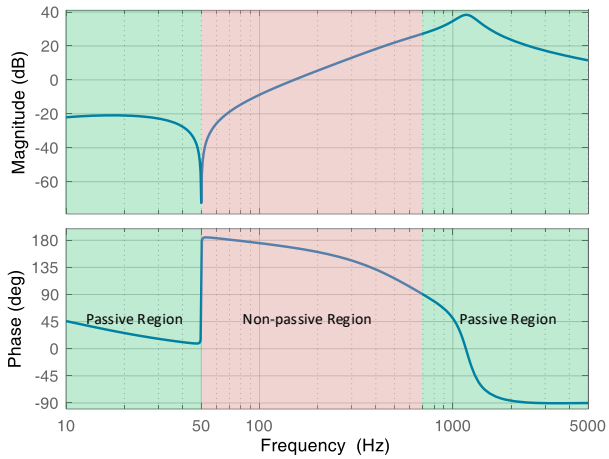

Fig. 8. The Bode diagram of the output impedance of the inverter.

The closed-loop system was investigated from the stability point of view in Section III. In the following, the output impedance of the inverter will be analyzed. An inverter with a pure capacitive output impedance, for example, may make the system unstable while it is connected to a pure inductive grid impedance or load. Therefore, the control system of the inverter should be designed to have a resistive behavior in all or at least a wide range of frequencies. In this way, the output impedance of the inverter has a passive behavior, and therefore, the inverter can work stably regardless of the behavior of the other components in the system. This is a simple definition of the passivity of the inverter. For a more detailed definition, the passivity theory suggests that the phase of the output impedance should be in the range of [-90°, 90°] [24]. In this condition, the inverter has always a positive real value that is the synonym of positive resistance. Otherwise, the negative resistance of the output impedance may make the system unstable depending on the load and grid conditions.

To investigate the behavior of the output impedance in different frequencies, it is extracted from Fig. 5 as follows:

$$Z_o(s) = \left.\frac{v_c(s)}{-i_o(s)}\right|_{v_{ref}=0} = \frac{Z_{L1}(s)Z_C(s)}{Z_{L1}(s)+Z_C(s)+G_V(s)G_{ap}(s)G_d(s)Z_C(s)} \tag{22}$$

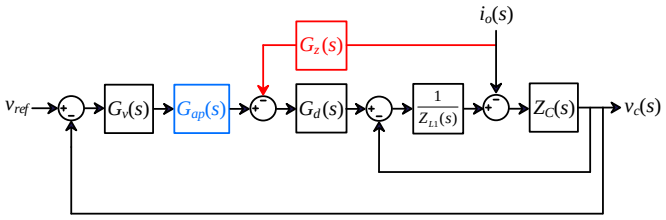

Fig. 9. The proposed control system for single-loop GFIs with an all-pass filter and output current feedback.

The Bode diagram of the output impedance of the inverter is presented in Fig. 8. As could be seen, in a wide range, which is shown in red in the figure, the phase of $Z_o(s)$ is more than 90°. In this region, the inverter has a resistive-inductive behavior, while its resistive part is negative. Therefore, if the inverter supplies a capacitive load while their impedances intersect in this region, the system will lose its stability. It is worth mentioning that regarding Fig. 7, the impedance Z_{L2} is a component of the grid/load impedance. In this way, Z_{L2} can affect the system stability by changing the load/grid impedance.

To make the output impedance passive, the control block diagram of Fig. 9 is proposed in which the inverter output current is adopted and fed through the controller $G_z(s)$ to the control system. In this condition, the modified output impedance of the inverter is given by

$$Z_{o,m}(s)=\frac{Z_{L1}(s)Z_C(s)+G_z(s)G_d(s)Z_C(s)}{Z_{L1}(s)+Z_C(s)+G_V(s)G_{ap}(s)G_d(s)Z_C(s)} \quad (23)$$

By comparing (22) and (23), it could be realized that only the numerator of the output impedance has been changed. Regarding Fig. 8, there should be a reduction in the phase of $Z_o(s)$ in the non-passive region. To this end, a lead-lag filter is used as given in (24), to introduce a negative phase to $Z_{o,m}(s)$ in the non-passive region.

$$G_z(s)=k_z\frac{s+\omega_z}{s+\omega_p} \quad (24)$$

In (24), k_z, ω_z, and ω_p are the controller's coefficient, zero angular frequency, and pole angular frequency, respectively. ω_z and ω_p should be tuned in the vicinity of the non-passive region, and also, ω_z should be larger than ω_p to introduce a negative phase to $Z_o(s)$. In this view, $\omega_z = 2\pi\times800$ and $\omega_p = 2\pi\times200$ are selected.

Fig. 10 could be used for tuning k_z, in which the phase of $Z_{o,m}(s)$ is plotted versus k_z and frequency. As could be realized, for $k_z \geq 3$, the phase of the output impedance is kept in the range of [-90°, 90°] up to the Nyquist frequency ($f_s/2$). Therefore, $k_z = 3$ is selected. The Bode diagram of $Z_{o,m}(s)$ with $k_z = 3$ is plotted in Fig. 11. It could be seen that unlike Fig. 8, the non-passive region is mitigated completely by employing the lead-lag filter. In this way, the system will retain its passivity, and the output impedance of the inverter will have a resistive behavior, ensuring system stability under different loads/grid impedances.

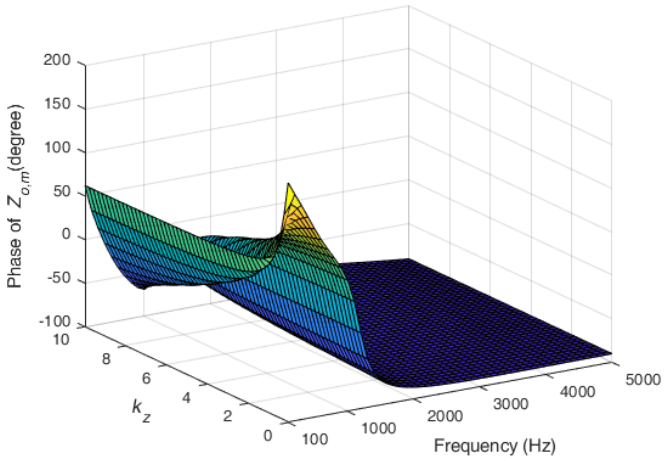

Fig. 10. The phase of the modified output impedance versus k_z and frequency.

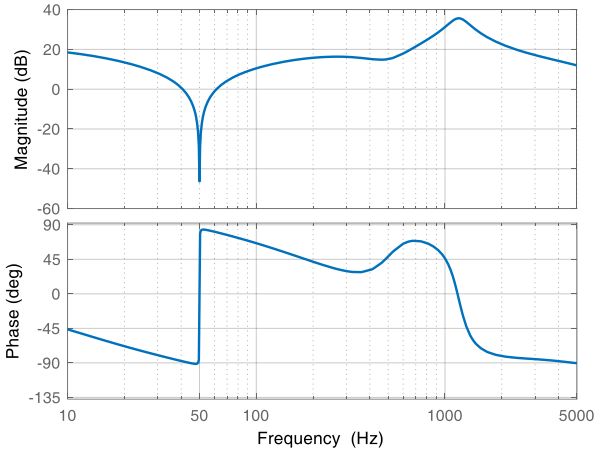

Fig. 11. The Bode diagram of the modified output impedance $Z_{o,m}(s)$.

V. Experimental Results

In this part, experiments are conducted to verify the validity of the proposed control system and its effectiveness in both grid-tied and off-grid modes. To this end, a small-scale setup is built in the lab, where similar system and control parameters to Table I are used. In order to implement the control system digitally, *dSPACE* DS1006 is employed. Grid-tied tests are also conducted using a *Chroma* 61845 grid simulator.

A. Grid-Tied Mode

To show the necessity of widening the stability region of the closed-loop system, a test is carried out in the grid-tied mode. The single-loop GFI was shown in Fig. 6 to be stable by using an all-pass filter when the resonance frequency is lower than $f_s/3$. To validate the correctness of this analysis, the inverter is connected to *Chroma* and injects power into the grid. Then, the all-pass filter is removed suddenly. Fig. 12 presents the inverter output current in this case. As could be observed, a clean and stable current is injected into the grid by the inverter while the all-pass filter is used. However, by

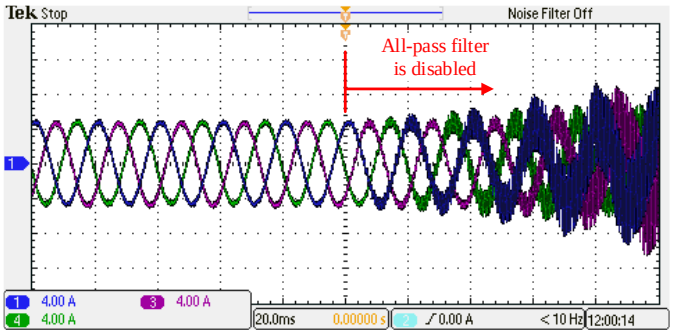

Fig. 12. The inverter output current in the grid-tied mode.

disabling the all-pass filter, the system becomes immediately unstable since the resonance frequency (f_r = 1250 Hz) is lower than $f_s/3$.

The conducted test illustrates the correlation between the experimental results and the theoretical analysis of Fig. 6. It also reveals that the stability region of the closed-loop system could be widened by introducing the negative phase to the system. In this way, the system is able to work stably without using resonance damping methods. In this regard, the all-pass filter has a very good potential to introduce the negative phase to the system without affecting the magnitude of the loop gain.

B. Off-Grid Mode

The experimental test is carried out in this part in the off-grid mode to show the necessity of the passivity of $Z_o(s)$. To this end, the inverter is connected to a parallel *RC* load, in which R = 80 Ω, C = 30 μF. Fig. 13 illustrates the Bode diagram of the output impedance of the inverter $Z_o(s)$ while $G_z(s)$ = 0, as well as the Bode diagram of the load impedance. It is worth mentioning that according to Fig. 7, the impedance Z_{L2} is considered as a part of the load impedance, i.e., $Z_{load} = Z_{L2} + Z_{R||C}$.

In accordance with impedance-based stability [12], the connection of two stable subsystems is stable if the PM is positive where their impedances intersect at the frequency f_{int}, in which

$$\mathrm{PM} = 180° - \left| \angle Z_o(f_{int}) - \angle Z_{load}(f_{int}) \right|. \tag{25}$$

According to (25), as the phase of the passive loads is always within [-90°, 90°], the PM will be always positive if the output impedance $Z_o(s)$ is passive. This is, however, not the case in Fig. 13. In this figure, it can be seen that the first intersection point occurs in the non-passive zone in which the phase of $Z_o(s)$ is beyond 90°, and consequently, results in a negative PM (PM = -27°). It, in turn, reveals that by connecting the system to the parallel *RC* load, it will be unstable.

Next, the output impedance of the inverter is made passive through output current feedback. Fig. 14 depicts the Bode diagrams of the load impedance and modified output impedance $Z_{o,m}(s)$. Contrary to the previous case, it is evident that whenever there is an intersection, the PM is always positive, which shows that the system can work stably in this condition.

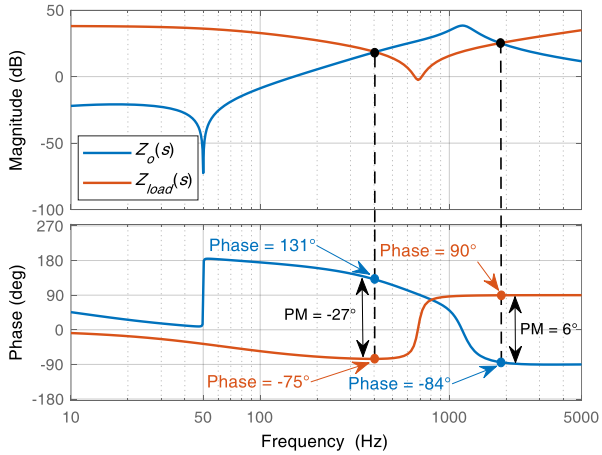

Fig. 13. The Bode diagrams of the output impedance without the output current feedback and load impedance.

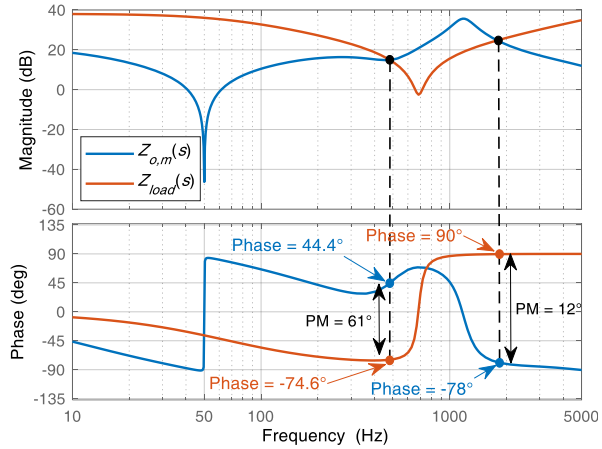

Fig. 14. The Bode diagrams of the output impedance using output current feedback and the load impedance.

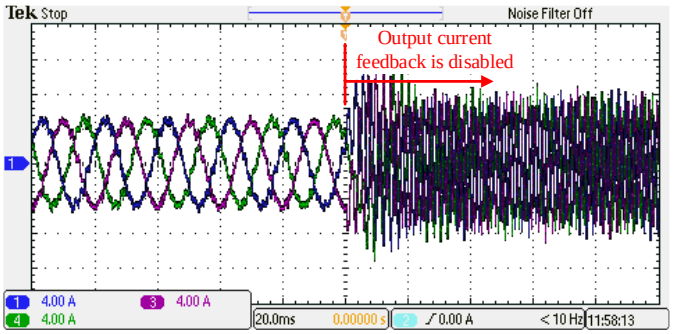

Fig. 15. The inverter output current in the off-grid mode.

To validate the analysis of Figs. 13 and 14, an experiment test is carried out in which the inverter has been connected to the *RC* load, while the output current feedback has been employed. Then, the output current feedback is disabled suddenly to show the consequence of the non-passivity of $Z_o(s)$. Fig. 15 shows the inverter output current in this case. It is evident that the inverter is stable at first, however, it becomes unstable immediately after disabling the output current feedback. The following should be noted because of

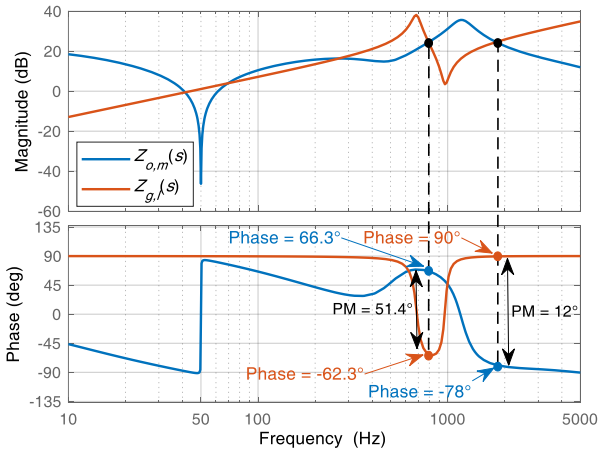

Fig. 16. The Bode diagrams of the modified output impedance and equivalent grid impedance.

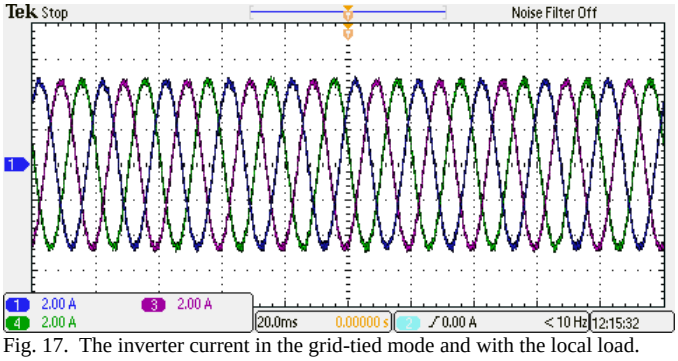

Fig. 17. The inverter current in the grid-tied mode and with the local load.

the relatively large capacitor in the load, a part of harmonic components passes through the load, and therefore, the load current has some harmonic contents before disabling the output current feedback. Nevertheless, the system is evidently stable in comparison with the case where the output current feedback is disabled. According to the experimental results presented in this section the passivity of the output impedance is as necessary as the stability of the closed-loop system.

C. Presence of the Local Load in the Grid-Tied Mode

In the following, a parallel *RC* load is connected to the inverter as a local load, while the inverter is connected to the grid. Referring to Fig. 7, the equivalent grid impedance in this condition is $Z_{g,l}(s) = Z_{L2} + [Z_{load}(s) \parallel Z_g(s)]$. Fig. 16 shows the Bode diagrams of the modified output impedance $Z_{o,m}(s)$ and equivalent grid impedance $Z_{g,l}(s)$. In view of the inverter's passivity of the output impedance, the PM at all intersection points is positive. The inverter output current is presented in Fig. 17, which is compatible with Fig. 16 and shows the stability of the whole system.

D. Transient Response

The transient response of the system is investigated in the grid-tied mode during the grid voltage disturbance. To this end, a 10% voltage drop is suddenly applied to the voltage grid using the grid simulator *Chroma*. Fig. 18 shows the inverter output current in this condition. As could be observed,

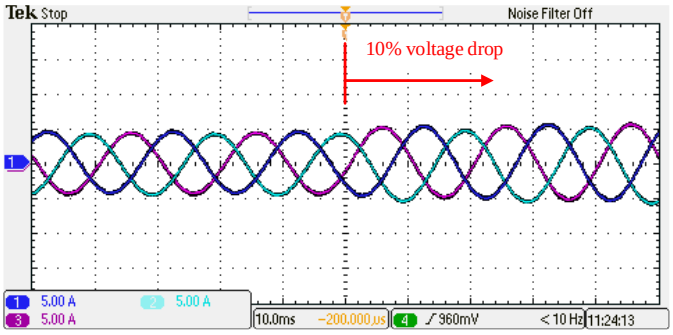

Fig. 18. The transient response of the system during grid voltage disturbance.

the system faces a small transient when the voltage drops. However, this transient is negligible which in turn shows the acceptable performance of the system in transient conditions.

VI. Conclusion

A method for extending the stability region of the closed-loop system in single-loop GFIs was proposed in this paper, which is based on the all-pass filter and injecting a negative phase into the system. In this way, the critical frequency is extended from $f_s/3$ to frequencies lower than $f_s/6$. After that, the output current feedback was utilized to make the output impedance passive. The method's validity was demonstrated by experiments in different scenarios.

References

[1] Q. C. Zhong and T. Hornik, "Cascaded current-voltage control to improve the power quality for a grid-connected inverter with a local load," *IEEE Trans. Ind. Electron.*, vol. 60, no. 4, pp. 1344–1355, Apr. 2013.

[2] K. Sung-Hun, H. Dehbonei, and C. V. Nayar, "Application of voltage and current-controlled voltage source inverters for distributed generation systems," *IEEE Trans. Energy*, vol. 21, no. 3, pp. 782–792, Sep. 2006.

[3] X. Li, P. Lin, Y. Tang, and K. Wang, "Stability design of single-loop voltage control with enhanced dynamic for voltage-source converters with a low *LC*-resonant-frequency," *IEEE Trans. Power Electron.*, vol. 33, no. 11, pp. 9937-9951, 2018.

[4] P. C. Loh and D. G. Holmes, "Analysis of multiloop control strategies for *LC*/*CL*/*LCL*-filtered voltage-source and current-source inverters," *IEEE Trans. Ind. Appl.*, vol. 41, no. 2, pp. 644–654, Mar./Apr. 2005.

[5] Y. Geng, Y. Yun, R. Chen, K. Wang, H. Bai and X. Wu, "Parameters design and optimization for *LC*-type off-grid inverters with inductor-current feedback active damping," *IEEE Trans. Power Electron.*, vol. 33, no. 1, pp. 703-715, Jan. 2018.

[6] Z. Zhao, Z. Han, X. Liu, J. Yao, B. Ji, S. Wang, et al., "Optimal tuning of the current loop for dual-loop controlled grid-forming converters based on active damping optimization," *IEEE Access*, vol. 9, pp. 35801-35813, 2021.

[7] A. Akhavan, S. Golestan, J. C. Vasquez, and J. M. Guerrero, "Passivity enhancement of voltage-controlled inverters in grid-connected microgrids considering negative aspects of control delay and grid impedance variations," *IEEE J. Emerg. Sel. Topics Power Electron.*, vol. 9, no. 6, pp. 6637-6649, Dec. 2021.

[8] X. Wang, F. Blaabjerg, and P. C. Loh, "Virtual *RC* damping of *LCL*-filtered voltage source converters with extended selective harmonic compensation," *IEEE Trans. Power Electron.*, vol. 30, no. 9, pp. 4726–4737, Sep. 2015.

[9] A. Akhavan, H. R. Mohammadi, J. C. Vasquez, and J. M. Guerrero, "Passivity-based design of plug-and-play current-controlled grid-

connected inverters," *IEEE Trans. Power Electron*, vol. 35, no. 2, pp. 2135-2150, Feb. 2020.
[10] Z. Xin, X. Wang, P. C. Loh, and F. Blaabjerg, "Grid-current-feedback control for *LCL*-filtered grid converters with enhanced stability," *IEEE Trans. Power Electron.*, vol. 32, no. 4, pp. 3216-3228, Apr. 2017.
[11] V. Miskovic, V. Blasko, T. M. Jahns, A. H. C. Smith, and C. Romenesko, "Observer-based active damping of *LCL* resonance in grid-connected voltage source converters," *IEEE Trans. Ind. Appl.*, vol. 50, no. 6, pp. 3977-3985, Nov./Dec. 2014.
[12] J. Sun, "Impedance-based stability criterion for grid-connected inverters," *IEEE Trans. Power Electron.*, vol. 26, no. 11, pp. 3075-3078, Nov. 2011.
[13] L. Harnefors, X. Wang, A. Yepes, and F. Blaabjerg, "Passivity-based stability assessment of grid-connected VSCs—An overview," *IEEE J. Emerg. Sel. Topics Power Electron.*, vol. 4, no. 1, pp. 116–125, Mar. 2016.
[14] X. Wang, P. C. Loh and F. Blaabjerg, "Stability analysis and controller synthesis for single-loop voltage-controlled VSIs," *IEEE Trans. Power Electron.*, vol. 32, no. 7, pp. 7394-7404, Sep. 2017.
[15] Z. Li, Y. Li, P. Wang, H. Zhu, C. Liu, and F. Gao, "Single-loop digital control of high-power 400-Hz ground power unit for airplanes," *IEEE Trans. Ind. Electron.*, vol. 57, no. 2, pp. 532–543, Feb. 2010.
[16] R. Peña-Alzola, M. Liserre, F. Blaabjerg, R. Sebastián, J. Dannehl, and F. W. Fuchs, "Analysis of the passive damping losses in *LCL*-filter-based grid converters," *IEEE Trans. Power Electron.*, vol. 28, no. 6, pp. 2642-2646, Jun. 2013.
[17] R. Turner, S. Walton, and R. Duke, "Robust high-performance inverter control using discrete direct-design pole placement," *IEEE Trans. Ind. Electron.*, vol. 58, no. 1, pp. 348–357, Jan. 2011.
[18] J. C. Vasquez, J. M. Guerrero, M. Savaghebi, J. Eloy-Garcia, and R. Teodorescu, "Modeling, analysis, and design of stationary-reference-frame droop-controlled parallel three-phase voltage source inverters," *IEEE Trans. Ind. Electron.*, vol. 60, no. 4, pp. 1271-1280, Apr. 2013.
[19] S. Buso and P. Mattavelli, *Digital Control in Power Electronics*, San Rafael, CA, USA: Morgan & Claypool Publ., 2006.
[20] A. Kuperman, "Proportional-resonant current controllers design based on desired transient performance," *IEEE Trans. Power Electron.*, vol. 30, no. 10, pp. 5341-5345, Oct. 2015.
[21] Y. Liao, X. Wang, and F. Blaabjerg, "Passivity-based analysis and design of linear voltage controllers for voltage-source converters," *IEEE Open J. Ind. Electron. Soc.*, vol. 1, pp. 114-126, 2020.
[22] J. L. Agorreta, M. Borrega, J. López, and L. Marroyo, "Modeling and control of *N*-paralleled grid-connected inverters with *LCL* filter coupled due to grid impedance in PV plants," *IEEE Trans. Power Electron.*, vol. 26, no. 3, pp. 770-785, Mar. 2011.
[23] X. Wang, F. Blaabjerg, and P. C. Loh, "Passivity-based stability analysis and damping injection for multiparalleled VSCs with *LCL* filters," *IEEE Trans. Power Electron*, vol. 32, no. 11, pp. 8922-8935, Nov. 2017.
[24] L. Harnefors, A. G. Yepes, A. Vidal, and J. Doval-Gandoy, "Passivity-based controller design of grid-connected VSCs for prevention of electrical resonance instability," *IEEE Trans. Ind. Electron.*, vol. 62, no. 2, pp. 702-710, Feb. 2015.

Ali Akhavan (Senior Member, IEEE) received the B.S., M.S., and Ph.D. degrees in electrical engineering from University of Kashan, Kashan, Iran in 2012, 2014, and 2019, respectively. Since August 2019, he has been with Aalborg University, Aalborg, Denmark, where he is currently a Postdoctoral Fellow with the AAU Energy. His research interests include power electronics, modeling and control of power converters, stability analysis, and microgrid clusters.

Juan C. Vasquez (Senior Member, IEEE) received the B.S. degree in electronics engineering from the Autonomous University of Manizales, Manizales, Colombia, in 2004, and the Ph.D. degree in automatic control, robotics, and computer vision from BarcelonaTech-UPC, Spain, in 2009. He was Assistant Professor and Associate Professor with the AAU Energy, Aalborg University, Denmark, in 2011 and 2014, respectively. In 2019, he became Professor in energy internet and microgrids. Currently, he is the Co-Director of the Villum Center for Research on Microgrids (CROM). He was a Visiting Scholar with the Center of Power Electronics Systems (CPES), Virginia Tech, U.S.A. and a Visiting Professor with Ritsumeikan University, Japan. He has published more than 450 journal papers in the field of microgrids, which in total are cited more than 19000 times. His current research interests include operation, advanced hierarchical and cooperative control, optimization, and energy management applied to distributed generation in ac/dc microgrids, maritime microgrids, advanced metering infrastructures, and the integration of Internet of Things and energy Internet into the SmartGrid.

Josep M. Guerrero (Fellow, IEEE) received the B.S. degree in telecommunications engineering, the M.S. degree in electronics engineering, and the Ph.D. degree in power electronics from the Technical University of Catalonia, Barcelona, Spain, in 1997, 2000, and 2003, respectively. Since 2011, he has been a Full Professor with the AAU Energy, Aalborg University, Aalborg, Denmark, where he is responsible for the Microgrid Research Program. From 2014, he has been a Chair Professor with Shandong University; from 2015, he has been a Distinguished Guest Professor with Hunan University; and from 2016, he has been a Visiting Professor Fellow with Aston University, Birmingham, U.K.; and a Guest Professor with the Nanjing University of Posts and Telecommunications, Nanjing, China. From 2019, he has been a Villum Investigator by The Villum Fonden, Søborg, Denmark, which supports the Center for Research on Microgrids (CROM), Aalborg University, being the founder and Director of the same center. His research interests include different microgrid aspects, including power electronics, distributed energy-storage systems, hierarchical and cooperative control, energy management systems, smart metering, and the Internet of Things for ac–dc microgrid clusters and islanded minigrids. He has authored or coauthored more than 600 journal papers in the fields of microgrids and renewable energy systems, which are cited more than 50000 times. His research specially focuses on microgrid technologies applied to offshore wind, maritime microgrids for electrical ships, vessels, ferries and seaports, and space microgrids applied to nanosatellites and spacecrafts.